Research Article | Vol. 11, No. 10 / 1 October 2020 / Biomedical Optics Express 6038
Biomedical Optics EXPRESS

Qualitative disorder measurements from backscattering spectra through an optical fiber

R. Fernández,[1,2,*] A. Marcos-Vidal,[1] S. Gallego,[2] A. Beléndez,[2] M. Desco,[1,3,4,5] and J. Ripoll[1,3]

[1]Departamento de Bioingeniería e Ingeniería Aeroespacial, Universidad Carlos III de Madrid, Madrid, Spain
[2]I.U. Física Aplicada a las Ciencias y las Tecnologías, Universidad de Alicante, Alicante, Spain
[3]Instituto de Investigación Sanitaria Gregorio Mara nón, Madrid, Spain
[4]Centro de Investigación Biomédica en Red de Salud Mental (CIBERSAM), Spain
[5]Centro Nacional de Investigaciones Cardiovasculares Carlos III (CNIC), Madrid, Spain
*robferna@ing.uc3m.es

Abstract: In the processes related to the development of cancer, there are different genetic and epigenetic events involved that result in structural changes of the affected cells. In the early stages of the disease, these changes occur at the nanoscale, remaining undetectable by conventional light microscopy, due to diffraction-limited resolution (~250 - 550 nm). In this sense, a technique termed partial wave spectroscopy (PWS) allows the detection of these nanostructural changes by measuring a statistical parameter called disorder strength (L_d). PWS uses a combination of a tunable filter and a camera to acquire the backscattering spectra for each pixel on the image. In this paper, we study and validate the possibility of obtaining a qualitative measurement of the disorder using the spectrum of the averaged spatial information. Instead of using spatial information and measuring sequentially spectral ranges, we measure the backscattered signal gathered by an optical fiber by means of a spectrograph. This will allow this method to be applied in systems where it is not possible to acquire a complete high resolution image for many spectral bands, while significantly enhancing speed.

1. Introduction

Although it can not be observed through conventional microscopy, healthy tissue suffers from different alterations before the development of a tumor, the so-called *field cancerization* [1]. The term refers to the presence of transformed cell primary tumors or abnormal tissue surrounding the cancerous region. It is related to the disease progression and relapse, involving multiple molecular events prior to tumor initiation and migration. This effect has been observed in nearly all kind of tissues present in the different organ systems of the human body [2]. A method able to detect these nanoscale changes, before the development of a tumor, is paramount in order to prevent and prematurely treat diseases in which the reaction time is a main factor [3]. In developed stages it has also a prime importance, helping to monitor tumor progression and defining tumor margins [4].

In this sense, electron microscopy (EM) has been studied for years as a support technique for light microscopy in tumor diagnosis [5,6]. Despite the fact that this technique allows the study of the structural features of the cell at nanoscale [7–9], it has important drawbacks. Among these drawbacks are the elevated cost of the instrument and its size, the regular power consumption, high degree of maintenance, researcher training and image artifacts resulting from sample preparation [10,11]. In light of this scenario, it is necessary to count on a more functional and versatile system to evaluate the nanostructure of cell, even *in vivo*, with minimum tissue preparation. Thus, a technique known as partial wave spectroscopy (PWS), introduced by V. Backman et al., has been recently developed and validated [12–19].

#396013 https://doi.org/10.1364/BOE.396013
Journal © 2020 Received 23 Apr 2020; revised 19 Sep 2020; accepted 19 Sep 2020; published 1 Oct 2020

Biomedical Optics EXPRESS

PWS is based on the idea that the backscattering spectrum of a weakly disordered medium contains spectral fluctuations that can be used to quantify the disorder strength based on the refractive index fluctuations within the cell, n. At a given location within the cell, n is proportional to the local density of macromolecules with refraction increment, Δn, practically independent of chemical composition. Thus, the spatial variations of macromolecular density can be measured once the fluctuations of n are known, assuming these fluctuations are random and within a correlation distance l_c.

The acquired spectrum of backscattered light is the result of the interference between the scattering produced by all n variations within an intracellular volume and the reflection from the interface at the surface of the cell. The measured spectra is therefore formed by a subset of the scattered waves, considering each pixel in an image a $1D$ weakly disordered medium.

In this $1D$ weakly disordered medium, of length L, the probability density distribution of the reflectance fluctuations, R, follows a log-normal distribution (i.e. $\ln(R)$ is a Gaussian function) for all length scales of this scattering medium.

Making use of the expected distribution for the reflection fluctuation, $\langle R \rangle$, and applying mesoscopic light transport theory [20], an expression for the disorder strength, L_d, is obtained from the correlation of these fluctuations, $\langle C(\Delta k) \rangle$, for the wavenumber $k = 2\pi/\lambda$ [13,14].

$$L_d \simeq -\beta \frac{\langle R \rangle}{k_c^2} \frac{(\Delta k)^2}{\ln\langle C(\Delta k) \rangle} \tag{1}$$

where β is a calibration constant determined experimentally [14], and the value for k_c is chosen as the central wavenumber of the measured spectra, $k_c = 2\pi/\langle \lambda \rangle$. Finally, $(\Delta k)^2/\ln\langle C(\Delta k) \rangle$ is found by performing a linear fit of $\ln\langle C(\Delta k) \rangle$ *vs* $(\Delta k)^2$.

PWS method was initially applied by spatially scanning the slit of a spectrograph and imaging the slit into a CCD camera to acquire each pixel's 1D backscattering information. The data collection using this method took around 4 - 5 minutes for a field of view which includes a single cell [13,14]. In subsequent works, the acquisition was done by the combination of a liquid crystal filter and a CCD camera. Thus, the backscattered image of the cell is collected for a range between 400 - 700 nm, avoiding the need of point scanning the sample. This results in a faster acquisition rate, 4 - 5 s for a single field of view [21]. Despite of this and due to their characteristics, these approaches are not suitable to be implemented in systems where the space and conditions are restricted, such as in small fiber endoscopy. In this sense, we evaluate the possibility of using a setup based on an spectrometer to calculate the L_d parameter directly from the backscattering signal gathered by an optical fiber.

2. Methods

2.1. Theoretical model

The PWS technique [13–15] was followed to measure spectral fluctuations in the backscattering spectra to obtain the statistical parameter termed disorder strength (L_d). This technique expresses a 3D disordered medium as various parallel and spatially independent 1D channels, acquiring the 1D *reflection spectra fluctuation*, $R(k)$, where k is formed by the interference of light waves propagating in these 1D channels and back-reflecting. For each pixel (x, y), it is therefore obtained Δn^2 as the variance of refractive index fluctuations of Δn. In this way, a 2D map of the disorder strength, $L_d(x, y)$, can be constructed, showing the spatial distribution of the disorder in the image under analysis. $R(k)$ is computed from the intensity *vs* wavelength measurement, $I(k)$, for each pixel in an image. To obtain $R(k)$, the signal $I(k)$ is filtered out by using a low-pass Butterworth filter to remove high-frequency noise. The variations in the lamp spectrum, sample roughness and instrument artifacts are also filtered by fitting a low order polynomial, $I_p(k)$, to $I(k)$. The fluctuating part of the reflection coefficient, $R(k)$, is obtained as $R(k) = I(k) - I_p(k)$.

Biomedical Optics EXPRESS

We here include the derivation found in Refs. [13,14] in order to provide a more complete description of the method. In a scattering medium with low disorder ($R \ll 1$), the probability density distribution of R follows a log-normal distribution for all length scales. The ensemble average of the R distribution over the ensemble of 1D independent parallel disordered channels of length L is given by:

$$\langle R \rangle = \frac{1}{2}\left[\exp\left(4k^2 L_d L/n_0^2\right) - 1\right] \tag{2}$$

where n_0 represents the average refractive index of the medium, and L is the dimension along the direction of incident light propagation through the medium. It is assumed in Eq. (2) that $4k^2 L_d L/n_0^2 \ll 1$, since n_0 is in the order of 1.4 and therefore,

$$\langle R \rangle \simeq \frac{1}{2}\left(\frac{4k^2 L_d L}{n_0^2}\right) \simeq \frac{2k^2 L_d L}{n_0^2} \tag{3}$$

In this low scattering regime, Eq. (3) can be rewritten as:

$$\langle R \rangle \simeq \frac{L}{\xi} \tag{4}$$

being ξ the $1D$ scattering mean free path:

$$\xi \simeq \left(\frac{2k^2 L_d}{n_0^2}\right)^{-1} = \left(\frac{2k^2 \langle \Delta n^2 \rangle l_c}{n_0^2}\right)^{-1} \tag{5}$$

By using the auto-correlation function $\langle C(\Delta k)\rangle$:

$$\langle C(\Delta k)\rangle = \frac{\langle R(k)R(k+\Delta k)\rangle}{\langle R(k)R(k)\rangle}, \tag{6}$$

from mesoscopic theory, $\langle C(\Delta k)\rangle$ can be expressed as [20]:

$$\langle C(\Delta k)\rangle \simeq \exp\left(-(\Delta k)^2 f(L_d)\alpha L\right), \tag{7}$$

where α is a constant, with units of length, and $f(L_d)$ is a slowly varying function of L_d, which may be considered constant for the ranges of k taken into account. Using Eq. (7) and Eq. (3), the length L of the 1D system, which is unknown experimentally and directly related to the temporal coherence length of the source, is removed from the equation:

$$\ln\langle C(\Delta k)\rangle = -(\Delta k)^2 f(L_d)\alpha L; L = -\frac{1}{\alpha f(L_d)}\frac{\ln\langle C(\Delta k)\rangle}{(\Delta k)^2}. \tag{8}$$

Using the above, the mean reflectance fluctuation equation can be written as:

$$\langle R \rangle \simeq \frac{2k^2 L_d L}{n_0^2}; \langle R \rangle \cong -\frac{2k^2 L_d}{n_0^2}\frac{\ln\langle C(\Delta k)\rangle}{\alpha f(L_d)(\Delta k)^2}. \tag{9}$$

From the equation above, the disorder, L_d, is obtained as:

$$L_d \simeq -\frac{f(L_d)\alpha\langle R\rangle n_0^2}{2k^2}\frac{(\Delta k)^2}{\ln\langle C(\Delta k)\rangle}. \tag{10}$$

By grouping constants (and slowly varying functions), we obtain [14]:

$$L_d \simeq -\beta\frac{\langle R\rangle}{k^2}\frac{(\Delta k)^2}{\ln\langle C(\Delta k)\rangle} \tag{11}$$

where β is a calibration constant determined experimentally. Equation (11) has a $1/k^2$ dependence and $(\Delta k)^2/\ln\langle C(\Delta k)\rangle$ is found by performing a linear fit of $\ln\langle C(\Delta k)\rangle$ *vs* $(\Delta k)^2$.

Biomedical Optics EXPRESS

It is worth noting that the auto-correlation function $\langle C(\Delta k)\rangle$ is defined as:

$$\langle C(\Delta k)\rangle = \frac{\sum_{i=1}^{N}(R(k_i)R(k_i+\Delta k)}{\sum_{i=1}^{N}(R(k_i)R(k_i))} \tag{12}$$

and the mean reflection fluctuation $\langle R\rangle$ is defined as:

$$\langle R\rangle = \sqrt{\frac{1}{N}\sum_{i=1}^{N}(R(k_i)R(k_i))} \tag{13}$$

2.2. Experimental setup

In order to evaluate the application of L_d calculation method to the whole spectrum measured by a spectrometer, a dual setup, depicted in Fig. 1, was used. This setup allowed us to simultaneously perform measurements of the backscattering spectra using the two methods mentioned in the introduction section.

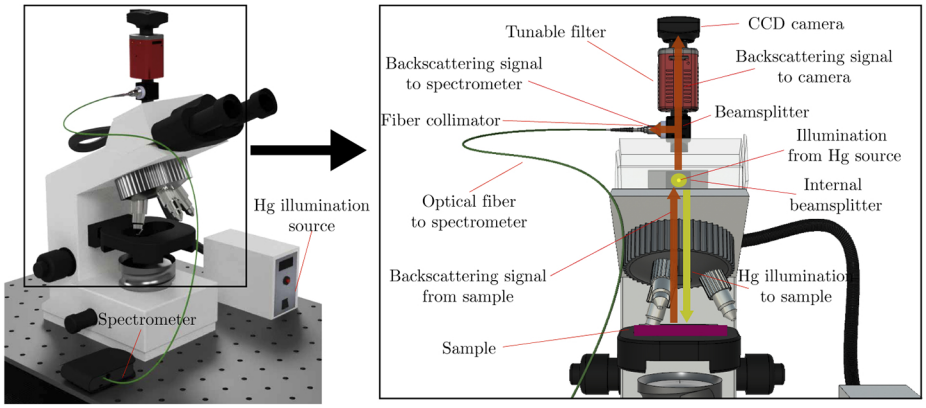

Fig. 1. Dual acquisition setup schematic.

2.2.1. Image based measurements

The first of these methods was implemented by using a combination of a Thorlabs Kurios WB1 tunable filter and a Thorlabs DCC1545M CCD camera to collect the backscattered light coming from a regular epi-fluorescence microscope, modified to acquire backreflected images from the sample. Through a internal beamsplitter, the light coming from a Hg lamp was guided to the sample (Fig. 2) . After illuminating the sample, the backscattering light passed again through the beamsplitter and it was directed to the CCD camera through the tunable filter. Thanks to the use of the tunable filter, it is possible to collect the backscattering intensity of a particular wavelength into the CCD camera without the need of perform a scan of the image pixel by pixel [21]. The range of the center wavelengths of tunable filter goes from 420 nm to 730 nm. Despite of this, the scan was performed from 500 nm to 650 nm to avoid being affected by noise due to low quantum efficiency wavelengths on CCD camera. The PWS technique was then followed to measure spectral fluctuations in the backscattering spectra to obtain the L_d parameter.

Biomedical Optics EXPRESS

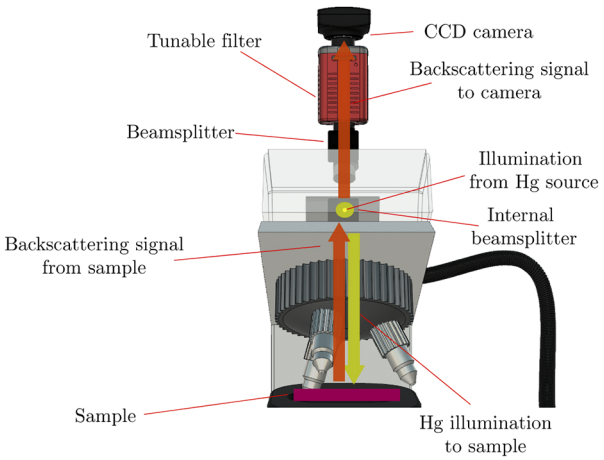

Fig. 2. Image based measurements setup, showing the light path followed by the Hg illumination to the sample and the path followed by the backscattering signal to the CCD camera.

2.2.2. Fiber based measurements

The second measuring method, through an optical fiber, is shown in Fig. 3. It was implemented to work simultaneously with the image based measurements, making use of a beamsplitter attached to the microscope output. The optical fiber was used to direct the backscattering light, collected by a fiber collimator, to a Hamamatsu C13555MA mini-spectrometer to measure the full spectrum of the backscattered light. In order to apply the PWS theory, the mean reflectance used to extract L_d parameter was calculated for a single mean intensity value for each wavelength instead of calculating it for each pixel. Thus, we have termed this disorder parameter as $\overline{L_d}$, which is a single-valued disorder parameter representing the mean disorder strength of the sample. Although it is not possible to construct a 2D map of the disorder strength, a qualitative parameter representing the mean disorder of the sample is obtained. To extract this parameter, the equations developed above (Eqs. (2) to (13)) were applied. This qualitative information, proportional to size and density of macromolecular architecture, allowed the separation of different tissue samples and different areas of the same tissue.

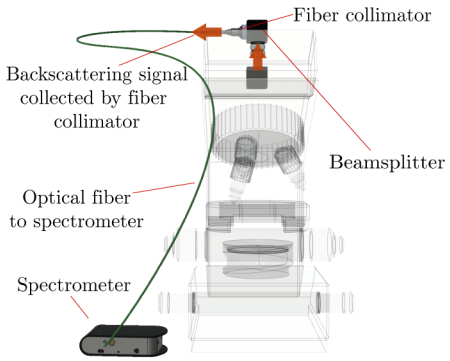

Fig. 3. Fiber based measurements setup. The light path and common parts have been intentionally omitted to shown in isolation the fiber based measurement module.

Biomedical Optics EXPRESS

3. Results and discussion

Different samples of thicknesses varying between 4 and 6 μm were measured using both methods simultaneously to compare the results and evaluate the similarities obtained. The samples used were histological sections of several healthy human tissue types, prepared with routine histological staining. A set of these samples is shown in Fig. 4. Using the setup described in Fig. 1, different areas of the same microscope slide containing the sample were measured. To determine the area seen by the fiber between each set of measurements, a laser beam was guided from the side of the spectrometer to the sample. Thus, the illuminated area showed the zone to be measured by the spectrometer. This area was a ~0.7 mm diameter circumference, as it is shown in Fig. 5. Then, the disorder parameter (L_d or $\overline{L_d}$) was obtained for each case using the methods already discussed. Since a 50:50 beamsplitter was employed, the intensity of the backscattered signal was halved. Despite of this, the illumination source provided good SNR in both the CCD camera and the spectrometer.

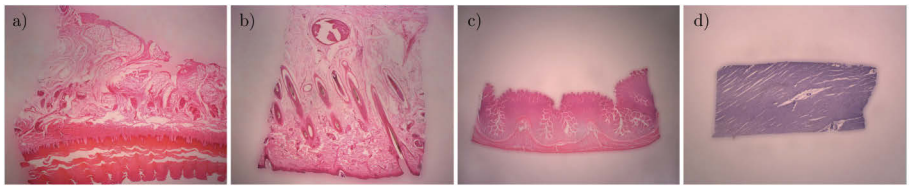

Fig. 4. Histological samples used for measurement's evaluation: a) Human skin (sample 1), b) Human skin (sample 2), c) Small intestine, d) Cardiac muscle. These images were obtained using an inverted microscope.

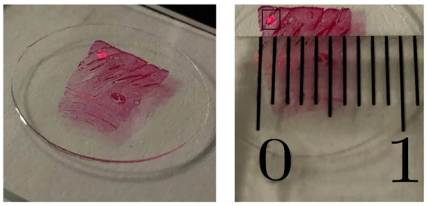

Fig. 5. Laser beam illuminating the area to be measured by the spectrometer. A circular zone of 0.7 mm diameter is measured using this method.

As mentioned above, each sample was divided in three zones (Zone A, Zone B, Zone C), each covering different regions of sample, as it is shown in Fig. 6 for a human skin sample. Then, the L_d and $\overline{L_d}$, obtained by each configuration respectively, were compared. In Fig. 7, the reflection coefficient R(λ) extraction procedure is depicted for both measurement methods. Disorder then is calculated from $\langle C(\Delta k)\rangle$ and $\langle R\rangle$ parameters. As it is shown in Fig. 8, $\langle C(\Delta k)\rangle$ has a (Δk^2) dependence.

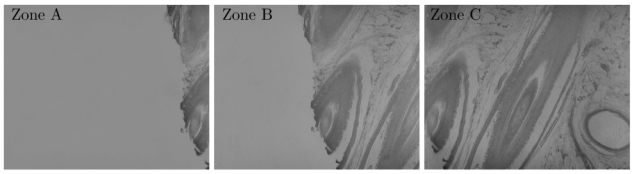

Fig. 6. Detail of the three measured zones in each sample. The images shown corresponds to Human skin (sample 1).

Biomedical Optics EXPRESS

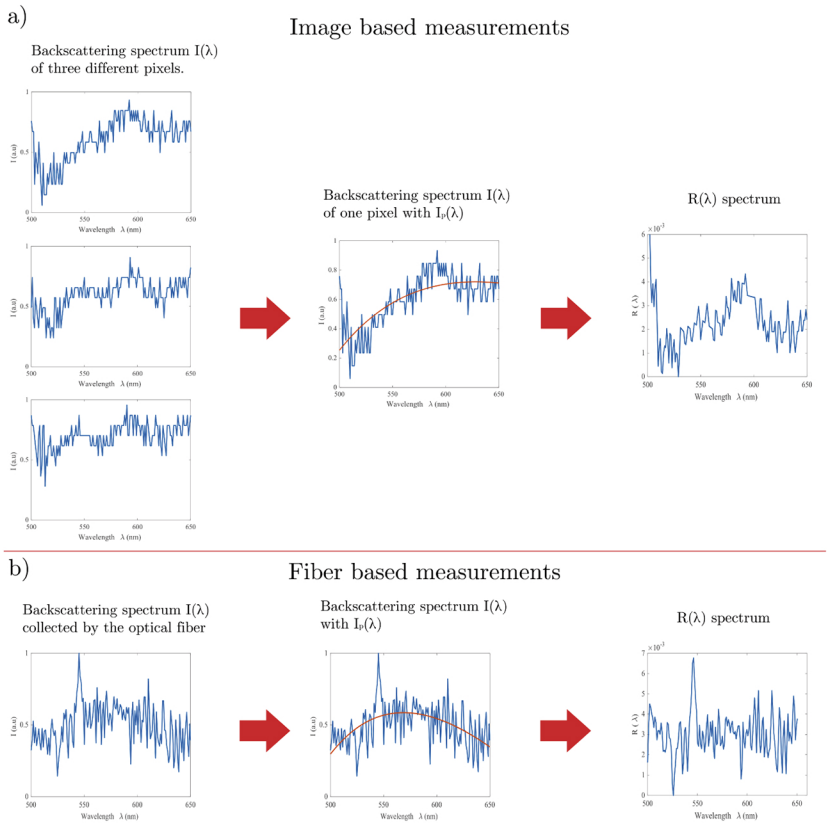

Fig. 7. Graphical example of reflection coefficient R(λ) extraction for human skin sample using the image based measurement method (a); and the fiber based measurement method (b). In (a), the backscattering spectrum I(λ) of three different pixels is shown. In the following steps, $I_p(\lambda)$ is shown in red over the backscattering spectrum for one pixel (a) and for the intensity gathered by the fiber (b) and then, the reflection coefficient R(λ) obtained in each case after removing the noise of the signals. Background reflection was previously removed in a) and b).

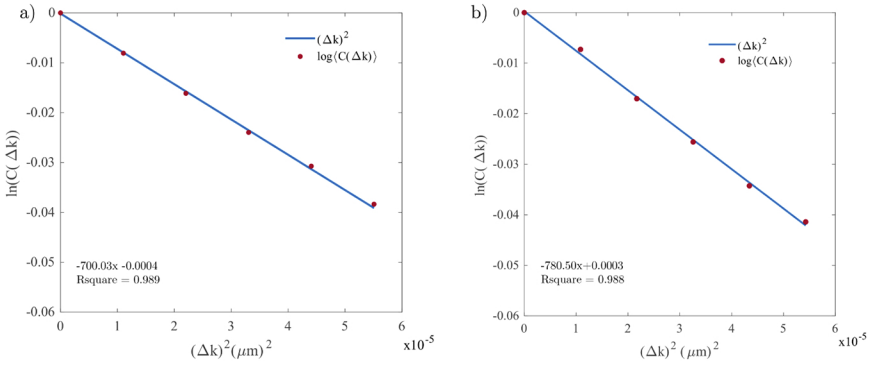

Fig. 8. The correlation decay showing the linear dependence of $\langle C(\Delta k)\rangle$ on (Δk^2). Measurements of Human Skin sample using a) image based method; b) fiber based method.

Biomedical Optics EXPRESS

Figure 9 shows the comparison between L_d and $\overline{L_d}$ parameters extracted from this human skin sample (sample 1) and the standard deviation of the disorders ($\sigma(L_d)$ and $\sigma(\overline{L_d})$) and the standard errors of each measurement, represented as a black line over each bar. The standard deviation follow similar variation than the disorder strength, as in [13,14].

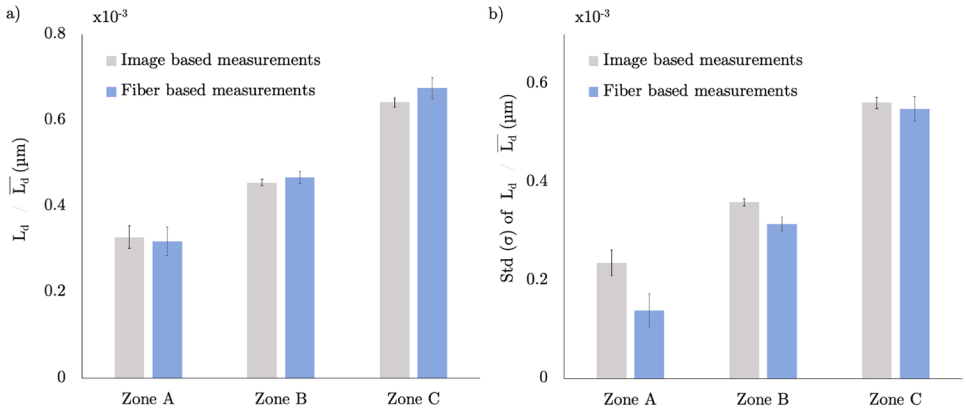

Fig. 9. Comparison of a) human skin sample's disorder obtained following PWS based on a CCD + tunable filter system (gray color) and using the mean value of each wavelength obtained by the spectrometer through the fiber (blue color); b) the standard deviation of L_d and $\overline{L_d}$ for each measurement method, respectively. Error bars are depicted in black over each measurement.

In the case of the image based method, the depicted L_d is the mean L_d for each zone. The standard error shown was also the one obtained for this mean disorder value. It can be seen how the values obtained through the fiber based method ($\overline{L_d}$) concur with the ones obtained through the image based method (L_d), showing the ability of the first to separate areas of the same sample with different disorder, which is lower for zones with less tissue presence and vice versa. The standard error obtained is slightly higher for fiber based measurements but it only represents around the 3% of the value of $\overline{L_d}$ obtained for Zones B and C. For Zone A, the error is higher in both methods, around 10%, but even in this case the error is sufficiently low to obtain qualitative differences between this zone and the other zones. Also, it is noticeable how the disorder value extracted from each zone is similar in both methods. The disorder obtained for each method and zone are detailed in Table 1.

Table 1. Disorder strength and standard error for both measurement methods

Measurement Method	Image based ($\mu m \cdot 10^{-3}$)		Fiber based ($\mu m \cdot 10^{-3}$)	
Zone	L_d	**Error**	$\overline{L_d}$	**Error**
Zone A	0.32813	0.02610	0.31891	0.03340
Zone B	0.45525	0.00732	0.46713	0.01406
Zone C	0.64194	0.01124	0.67471	0.02454

To evaluate the consistence of the proposed method obtaining $\overline{L_d}$ parameter, the measurement of zones with different sample presence was done for multiple samples. The samples and zones analyzed are shown in Fig. 10. As in the aforementioned measurements, for each sample, three different zones were measured (zones A, B and C). The same criteria was followed in all the different samples with respect to the areas measured: Zone A covered a small amount of sample, zone B covered medium amount of sample and zone C, a big amount of sample. The rest of the area measured was empty microscope slide.

Biomedical Optics EXPRESS

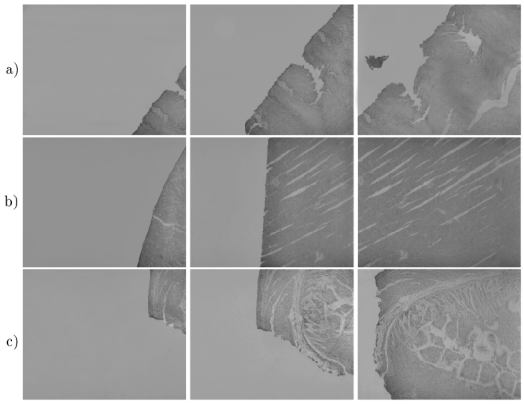

Fig. 10. Set of different tissue samples used, showing the areas measured: a) Human skin (sample 2), b) Cardiac muscle, c) Small intestine.

Fig. 11 shows the $\overline{L_d}$ calculated for these tissue samples following fiber based method. The results show how the method is able to separate the different areas of the samples attending to the different disorder of each zone. It is also capable of classifying the different healthy tissues regarding to their $\overline{L_d}$ parameter. The small intestine sample showed the lower values of disorder strength, followed by cardiac muscle sample.This is probably related to the higher heterogeneity of the selected skin samples when compared to the other two, which presents more homogeneous structures. In Table 2, $\overline{L_d}$ values obtained for each sample and zone are specified. Although the qualitative values obtained by the proposed method cannot be numerically compared to the ones obtained by original PWS method, the results were in accordance for different areas of the same sample.

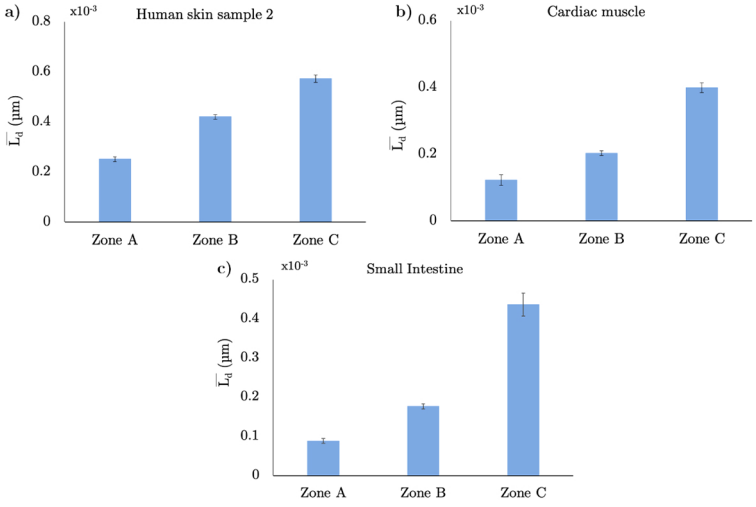

Fig. 11. $\overline{L_d}$ of three different samples obtained for three different zones of the microscope slide containing the sample, following fiber based method. a) Human skin (sample 2); b) Small intestine; c) Cardiac muscle.

Biomedical Optics EXPRESS

Table 2. $\overline{L_d}$ obtained for three zones in three different tissue samples (shown in Fig. 10): a) Human skin (sample 2) ; b) Cardiac muscle; c) Small intestine

	Sample $\overline{L_d}$ ($\mu m \cdot 10^{-3}$) and standard error ($\mu m \cdot 10^{-3}$)					
Zone	a)	Error	b)	Error	c)	Error
Zone A	0.25071	0.00929	0.12146	0.01574	0.08852	0.00601
Zone B	0.41923	0.00888	0.20272	0.00656	0.17667	0.00691
Zone C	0.57150	0.01474	0.39851	0.01464	0.43651	0.02914

4. Conclusion

An alternative method of applying the PWS technique by means of fiber-based measurements has been validated. This technique makes use of an optical fiber to guide the backscattered light from a sample to a spectrograph to analyze the whole spectrum and provides a spatially averaged value proportional to the field's of view present disorder. To validate the proposed method, a dual acquisition setup was implemented in a modified epi-fluorescence microscope. This setup allowed us to acquire the backscattering spectrum in a CCD camera and in a spectrometer, through an optical fiber. That was done simultaneously to compare the disorder strength extracted from the data measured by both methods in the same measurement conditions. For different samples, this alternative method is also able to separate zones with different tissue presence. A higher $\overline{L_d}$ value was obtained for areas located in the centre of the sample, where there was more presence of the tissue and, therefore, higher disorder. This methodology offers the possibility to compare the qualitative differences between samples and could be a potential useful tool to discriminate between different stages of disease. However, due to the fact that it is not strictly quantitative, it is not capable of providing a robust number that may be compared with other modalities yielding values related to sample density or mean free path.

Further validation of this method is necessary to be carried out. In particular, it is needed to evaluate its efficiency characterizing the same tissue in different stages of a particular disease, such as tumors. Despite of this, the flexibility given by the optical fiber used to gather the light together with the scanning speed and the results obtained in this first validation, opens up a way of implementing this small footprint measurement method in systems with limited space and restricted measurement conditions, such as endoscopes and other in-vivo detection systems.

Funding

Horizon 2020 Framework Programme (801347-SENSITIVE); Ministerio de Economía y Competitividad (FIS2016-77892-R); Conselleria d'Educació, Investigació, Cultura i Esport (APOSTD/2018/A/084); Comunidad de Madrid (S2017/BMD-3867 RENIM-CM); Ministerio de Ciencia, Innovación y Universidades (SEV-2015-0505).

Acknowledgments

This project is funded by the Horizon 2020 Framework Programme (801347-SENSITIVE), Ministerio de Economía y Competitividad (FIS2016-77892-R), Conselleria d'Educació, Investigació, Cultura i Esport and European Social Fund (APOSTD/2018/A/084), Comunidad de Madrid (S2017/BMD-3867 RENIMCM) and co-financed by European Structural and Investment Fund. CNIC is supported by Ministerio de Ciencia, Innovación y Universidades and the Pro CNIC Foundation, and is a Severo Ochoa Center of Excellence (SEV-2015-0505).

Disclosures

The authors declare that there are no conflicts of interest related to this article.

Biomedical Optics EXPRESS

References

1. D. P. Slaughter, H. W. Southwick, and W. Smejkal, "Field cancerization in oral stratified squamous epithelium. Clinical implications of multicentric origin," Cancer **6**(5), 963–968 (1953).
2. P. Lochhead, A. T. Chan, R. Nishihara, C. S. Fuchs, A. H. Beck, E. Giovannucci, and S. Ogino, "Etiologic field effect: Reappraisal of the field effect concept in cancer predisposition and progression," Mod. Pathol. **28**(1), 14–29 (2015).
3. J. A. O'Shaughnessy, G. J. Kelloff, G. B. Gordon, A. J. Dannenberg, W. K. Hong, C. J. Fabian, C. C. Sigman, M. M. Bertagnolli, S. P. Stratton, S. Lam, W. G. Nelson, F. L. Meyskens, D. S. Alberts, M. Follen, A. K. Rustgi, V. Papadimitrakopoulou, P. T. Scardino, A. F. Gazdar, L. W. Wattenberg, M. B. Sporn, W. A. Sakr, S. M. Lippman, and D. D. Von Hoff, "Treatment and prevention of intraepithelial neoplasia: an important target for accelerated new agent development," Clin. Cancer Res. **8**(2), 314–346 (2002).
4. G. D. Dakubo, J. P. Jakupciak, M. A. Birch-Machin, and R. L. Parr, "Clinical implications and utility of field cancerization," Cancer Cell Int. **7**(1), 2–12 (2007).
5. J. D. Elema and H. M. Keuning, "The use of electron microscopy for the diagnosis of cancer in bronchial biopsies," Hum. Pathol. **19**(3), 304–308 (1988).
6. N. G. Ordóñez and B. Mackay, "Electron microscopy in tumor diagnosis: Indications for its use in the immunohistochemical Era," Hum. Pathol. **29**(12), 1403–1411 (1998).
7. M. Dela Cruz, L. K. Bianchi, L. Cherkezyan, C. White, Y. Stypula-Cyrus, H. Subramanian, R. K. Wali, H. K. Roy, V. Backman, and M. J. Goldberg, "Nanoscale changes in chromatin organization represent the initial steps of tumorigenesis: a transmission electron microscopy study," BMC Cancer **14**, 189 (2014).
8. T. Okada and T. Ogura, "High-resolution imaging of living mammalian cells bound by nanobeads-connected antibodies in a medium using scanning electron-assisted dielectric microscopy," Sci. Rep. **7**(1), 43025–10 (2017).
9. Y. Zhang, T. Huang, D. M. Jorgens, A. Nickerson, L. J. Lin, J. Pelz, J. W. Gray, C. S. López, and X. Nan, "Quantitating morphological changes in biological samples during scanning electron microscopy sample preparation with correlative super-resolution microscopy," PLoS One **12**, e0176839 (2017).
10. B. Eyden, "Electron microscopy in the diagnosis of tumours," Curr. Diagn. Pathol. **8**(4), 216–224 (2002).
11. A. L. Robson, P. C. Dastoor, J. Flynn, W. Palmer, A. Martin, D. W. Smith, A. Woldu, and S. Hua, "Advantages and limitations of current imaging techniques for characterizing liposome morphology," Front. Pharmacol. **9**, 1–8 (2018).
12. Y. Liu, X. Li, Y. L. Kim, and V. Backman, "Elastic backscattering spectroscopic microscopy," Opt. Lett. **30**(18), 2445 (2005).
13. H. Subramanian, P. Pradhan, Y. Liu, I. R. Capoglu, X. Li, J. D. Rogers, A. Heifetz, D. Kunte, H. K. Roy, A. Taflove, and V. Backman, "Optical methodology for detecting histologically unapparent nanoscale consequences of genetic alterations in biological cells," Proc. Natl. Acad. Sci. **105**(51), 20118–20123 (2008).
14. H. Subramanian, P. Pradhan, Y. Liu, I. R. Capoglu, J. D. Rogers, H. K. Roy, R. E. Brand, and V. Backman, "Partial-wave microscopic spectroscopy detects subwavelength refractive index fluctuations: an application to cancer diagnosis," Opt. Lett. **34**(4), 518 (2009).
15. H. Subramanian, P. Viswanathan, L. Cherkezyan, R. Iyengar, S. Rozhok, M. Verleye, J. Derbas, J. Czarnecki, H. K. Roy, and V. Backman, "Procedures for risk-stratification of lung cancer using buccal nanocytology," Biomed. Opt. Express **7**(9), 3795 (2016).
16. Y. Stypula-Cyrus, D. Damania, D. P. Kunte, M. D. Cruz, H. Subramanian, H. K. Roy, and V. Backman, "HDAC Up-Regulation in Early Colon Field Carcinogenesis Is Involved in Cell Tumorigenicity through Regulation of Chromatin Structure," PLoS One **8**(5), e64600 (2013).
17. A. Eshein, Y. Li, X. Zhou, G. Spicer, T.-Q. Nguyen, L. M. Almassalha, J. E. Chandler, S. Gladstein, B. Dong, C. Sun, H. F. Zhang, and V. Backman, "Nanoscale Imaging of Chromatin with Labeled and Label-Free Super-Resolution Microscopy and Partial-Wave Spectroscopy," Biophotonics Congr. Biomed. Opt. Congr. 2018 (Microscopy/Translational/Brain/OTS) **2018**, MW2A.4 (2018).
18. S. Gladstein, D. Damania, L. M. Almassalha, L. T. Smith, V. Gupta, H. Subramanian, D. K. Rex, H. K. Roy, and V. Backman, "Correlating colorectal cancer risk with field carcinogenesis progression using partial wave spectroscopic microscopy," Cancer Med. **7**(5), 2109–2120 (2018).
19. L. M. Almassalha, G. M. Bauer, J. E. Chandler, S. Gladstein, L. Cherkezyan, Y. Stypula-Cyrus, S. Weinberg, D. Zhang, P. Thusgaard Ruhoff, H. K. Roy, H. Subramanian, N. S. Chandel, I. Szleifer, and V. Backman, "Label-free imaging of the native, living cellular nanoarchitecture using partial-wave spectroscopic microscopy," Proc. Natl. Acad. Sci. **113**(42), E6372–E6381 (2016).
20. P. Pradhan and N. Kumar, "Localization of light in coherenlty amplifying media," Phys. Rev. B **50**(13), 9644–9647 (1994).
21. D. Damania, H. Subramanian, A. K. Tiwari, Y. Stypula, D. Kunte, P. Pradhan, H. K. Roy, and V. Backman, "Role of cytoskeleton in controlling the disorder strength of cellular nanoscale architecture," Biophys. J. **99**(3), 989–996 (2010).